



# Ag Functionalized $\text{In}_2\text{O}_3$ Derived From MIL-68(In) as an Efficient Electrochemical Glucose Sensor

Dooa Arif<sup>1</sup>, Zakir Hussain<sup>1\*</sup>, Amna Didar Abbasi<sup>1</sup> and Manzar Sohail<sup>2</sup>

<sup>1</sup>Department of Materials Engineering, School of Chemical and Materials Engineering (SCME), National University of Sciences & Technology (NUST), Islamabad, Pakistan, <sup>2</sup>Department of Chemistry, School of Natural Sciences (SNS), National University of Sciences & Technology (NUST), Islamabad, Pakistan

In this study,  $\text{Ag@In}_2\text{O}_3$  modified nickel foam (NF) was reported for its role as a non-enzymatic glucose sensor.  $\text{Ag@In}_2\text{O}_3$  was prepared by a simple two-step method; preparation of a metal-organic framework (MOF) MIL-68(In) by solvothermal method, entrapment of Ag + by adding  $\text{AgNO}_3$  then drying it for 2 h to complete the entrapment process and subsequent calcination at  $650^\circ\text{C}$  for 3 h. The  $\text{Ag@In}_2\text{O}_3$  modified NF was employed as a non-enzymatic glucose sensor to determine glucose concentrations in an alkaline medium. Two linear ranges were obtained from  $\text{Ag@In}_2\text{O}_3$  modified electrode, i.e.,  $10\ \mu\text{M}$  to  $0.8\ \text{mM}$  and  $0.8\text{--}2.16\ \text{mM}$  with a sensitivity of  $3.31\ \text{mA}\ \text{mM}^{-1}\ \text{cm}^{-2}$  and  $1.51\ \text{mA}\ \text{mM}^{-1}\ \text{cm}^{-2}$  respectively, with a detection limit of  $0.49\ \mu\text{M}$ .  $\text{Ag@In}_2\text{O}_3$  modified NF exhibited high selectivity for glucose, among other interfering agents.

**Keywords:** glucose sensing, sensors, indium oxide, MIL-68(In), MOFs

## INTRODUCTION

Glucose fuels our bodies to sustain everyday activities and is an essential carbohydrate, but its high concentration leads to an increased risk of heart diseases and diabetes mellitus. Hence, it is crucial to quantify the amount of glucose in the blood, and it is a need of the hour to explore rapid and efficient sensors for the detection of glucose (Nichols et al., 2013; Yang and Gao, 2019). For this purpose, multiple efforts have been made academically, commercially, and industrially to develop an effective electrochemical enzymatic glucose sensor for medical diagnosis, research, and management of pharmaceuticals and food. Under mild conditions, two major natural enzymes, glucose oxidase and glucose dehydrogenase, show excellent selectivity towards glucose. They are extensively used in enzymatic glucose sensors as biological catalysts (Wang, 2008). Clark and Lyons (1962) were the first to introduce the concept of enzymatic glucose sensors (Clark and Lyons, 1962). However, enzyme-based sensors are expensive, chemically unstable, and sensitive to temperature, pH, and humidity.

Moreover, due to the difficulty in immobilization procedures of enzymes, research was then diverted to develop non-enzymatic glucose sensors having significant characteristics like stability, selectivity and sensitivity (Hwang et al., 2018). The most sensitive technique to detect glucose non-enzymatically is the electrochemical method based on electrocatalytic oxidation of glucose (Zhao et al., 2019). Fabrication of reliable, sensitive electrochemical sensors for biological analysis depends on the development of advanced electrocatalysts (Govindasamy et al., 2019). Recently, there has been growing attention towards metal-organic frameworks (MOFs) in electrochemical sensors' area because of their unique features like tunable structure, large surface area, and adjustable aperture (Song, 2017; Li J. et al., 2019). Metal-organic frameworks constructed of metal ions and organic ligands are proven to be exceptional materials for producing metal oxides with intriguing

## OPEN ACCESS

### Edited by:

Jennifer L. Schaefer,  
University of Notre Dame,  
United States

### Reviewed by:

Anirban Paul,  
The University of Texas at Dallas,  
United States  
Wei Meng,  
North China University of Science and  
Technology, China

### \*Correspondence:

Zakir Hussain  
zakir.hussain@scme.nust.edu.pk

### Specialty section:

This article was submitted to  
Electrochemistry,  
a section of the journal  
Frontiers in Chemistry

**Received:** 28 March 2022

**Accepted:** 19 April 2022

**Published:** 09 May 2022

### Citation:

Arif D, Hussain Z, Abbasi AD and  
Sohail M (2022) Ag Functionalized  
 $\text{In}_2\text{O}_3$  Derived From MIL-68(In) as an  
Efficient Electrochemical  
Glucose Sensor.  
Front. Chem. 10:906031.  
doi: 10.3389/fchem.2022.906031

microstructures (Cao et al., 2017). Metal oxides have a small specific surface area and are prone to agglomeration, contributing to undesirable electrochemical properties (Song et al., 2018). MOFs are used as a template to produce metal oxides. An effective strategy to increase metal oxides' surface area and stability is chemically and thermally treating MOFs (Chu et al., 2020). Furthermore, MOFs-derived metal oxides have a larger surface area and provide a simple route for the movement of ions and electrons. Similarly, their hollow structure aids in lowering stress over the electrode material during the charge and discharge process that enhances their electrochemical activity and cycling stability, increasing their suitability for sensing and supercapacitor applications (Song et al., 2015; Wang et al., 2015; Salunkhe et al., 2017). When used as a sacrificial template for producing porous metal oxides, MOFs, their low conductivity and poor resistance against acid-alkali corrosion are atoned while showing good stability and catalytic activity (Li L. et al., 2019). Because of their porosity, MOFs provide fast access to ions and molecules during the transformation process. Therefore, the functionalization of calcined MOFs intensifies the effective surface area and catalytic response for electrochemical sensors. For these reasons, MOFs have attracted much attention as a precursor for synthesizing nanocomposite metal oxides (Stock and Biswas, 2012; Lü et al., 2014). For instance, Wang J. et al. (2020) developed and reported an isoniazid sensor based on calcined Zn/Ni-MOF, resulting in higher catalytic activity than pristine MOF. Compared to the aggregated microsphere without growth templates, metal oxides derived from MOFs have more benefits, such as sufficient active surface area and favorable kinetics (Wei et al., 2020). Indium oxide (In<sub>2</sub>O<sub>3</sub>) is a prominent n-type semiconductor with a wide bandgap (e.g., 3.55–3.75 eV). In<sub>2</sub>O<sub>3</sub> has been frequently employed in many optic and electrical devices owing to its unique chemical properties (e.g., strong surface reactivity and high carrier conductivity) (Wang X. et al., 2020). MIL-68(In) is a type of MOF that can be easily synthesized in a non-aqueous medium using a solvothermal approach (Barthelet et al., 2004), and has emerged as a promising template for the production of porous nanostructure metal oxides (Wang et al., 2018; Zhang et al., 2019). The MILs, which are made up of metal-centered octahedra (MO<sub>4</sub>(OH)<sub>2</sub>, M = In, Ga, and Fe) and organic ligands like terephthalic acid, have a three-dimensional network structure with ultrahigh porosity (Volkringer et al., 2008). To generate metal doped In<sub>2</sub>O<sub>3</sub> porous nanostructures, selecting MILs with distinct metal-centered octahedrons as the precursor or self-sacrificial template is a simple and promising technique. The introduction of a few impurity ions during the pyrolysis process of the MILs precursor can limit the continued growth of the new material nanoparticles, resulting in a reduction in the particle size of sensing materials and an increase in the active sites for sensing reaction.

Moreover, in addition to MOFs, various other porous materials such as metal oxide (Sheng et al., 2016), graphene (Zhan et al., 2014), and conducting polymer foams (Sun et al., 2016) are also used as electrode material, reported in the literature. To this end, Nickel Foam (NF) is an electrode

with 3D porous structure and has the most significant current collecting properties. NF displays sizeable active surface area, good electrical conductivity, high flexibility and better mass transport properties, making it suitable to be used directly as an electrode material (Zhou et al., 2013). It has also been demonstrated that In<sub>2</sub>O<sub>3</sub>, when doped with metals and metal oxides, shows increased sensitivity and selectivity, and reduced working temperature, and decreased response and recovery time resulting in improved performance of the sensors (Liang et al., 2012). Similarly, silver (Ag) has also been used as a dopant material to provide a specific adsorption site for the adsorption of oxygen and analyte molecules which could potentially help the catalytic oxidation on the surface of sensing materials by activating the analyte (Wang et al., 2014).

Taking the above considerations into account, we have synthesized MOFs-derived porous and well-ordered Indium oxide and their composite with Ag<sup>+</sup> for glucose sensing. Herein, we propose the synthesis of porous In<sub>2</sub>O<sub>3</sub> by thermal decomposition of Indium organic frameworks (InOF). Two steps route was followed to prepare the porous In<sub>2</sub>O<sub>3</sub> and Ag@In<sub>2</sub>O<sub>3</sub>, i.e., formation of MIL-68(In) also known as Indium Organic Frameworks (InOFs) and then its calcination at 650°C.

## EXPERIMENTAL

### Reagents

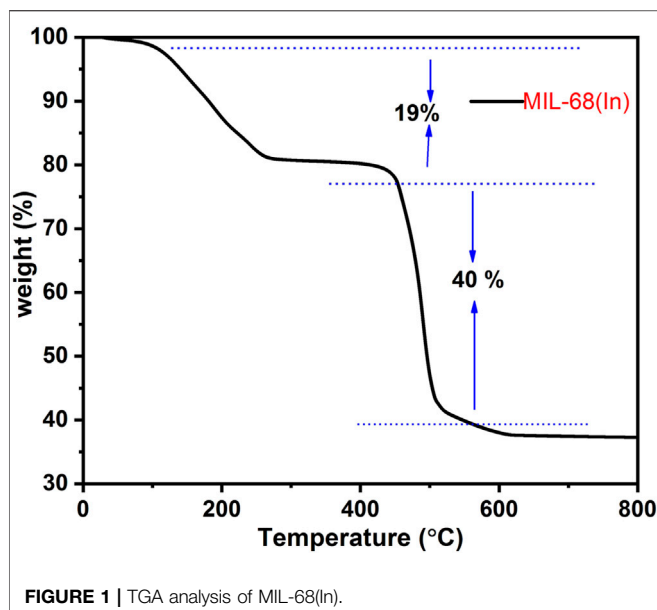
Materials including L (+)—Ascorbic acid and Terephthalic acid were bought from Merck KGaA, 64,271 Darmstadt Germany. Indium (III) nitrate hydrate and uric acid were purchased from SIGMA ALDRICH Co., United States. Silver nitrate was purchased from Duksan Pure Chemicals Co. Ltd. 635-1, KOREA. Dopamine hydrochloride was acquired from Solarbio. The purchased chemicals were not further purified and were used as received.

### Synthesis of MIL-68(In)

MIL-68(In) was prepared by following the protocols obtained from the literature (Volkringer et al., 2008). Briefly, (1.05 mmol, 408.2 g) indium nitrate was mixed with terephthalic acid (1.2 mmol, 200 mg), and DMF (70 mmol, 5 ml). This mixture was then shifted to Teflon-lined stainless-steel autoclave and placed in an oven at 100°C for 48 h. The resultant mixture was filtered and washed several times using DMF. After filtration, the resultant white precipitate was placed in a vacuum oven for 12 h at 80°C.

### Synthesis of Ag@In<sub>2</sub>O<sub>3</sub>

A two-step approach was used to prepare the Ag@In<sub>2</sub>O<sub>3</sub> combination, as described in the literature (Xue et al., 2017). Briefly, 20 mg of as-synthesized MIL-68(In) was weighed accurately and ground for 10 min in a mortar, followed by adding of AgNO<sub>3</sub> (5.4 × 10<sup>-2</sup> mol/L) solution into the finely ground InOF powder to obtain white pulp. The white pulp was set for drying in an oven at 60°C for 2 h to



complete the entrapment process. Finally, the synthesized Ag@InOF precursor was placed in the ceramic crucible in a muffle furnace for 3 h at 650°C to obtain Ag@In<sub>2</sub>O<sub>3</sub>.

### Fabrication of Ag@In<sub>2</sub>O<sub>3</sub> on Nickel Foam

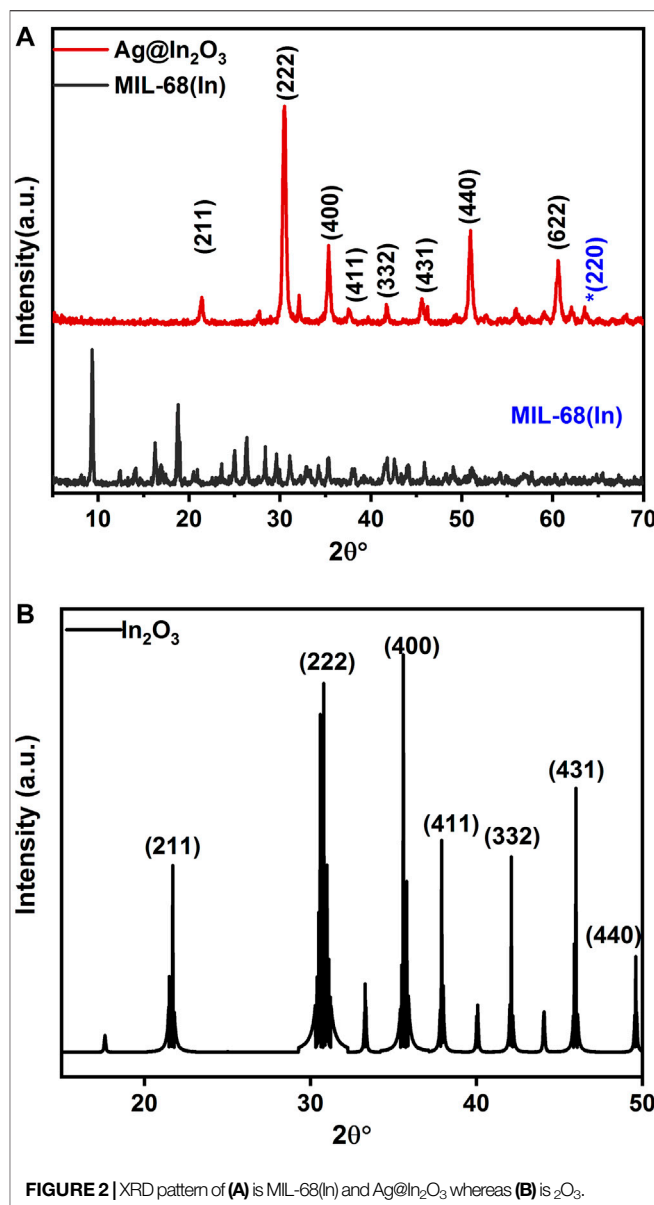
For electrode fabrication, 1 cm × 1 cm Nickel Foam (NF) was appropriately cleaned by immersing it in 3 M HCl and sonicated for 5 min. It was then washed with distilled water, sonicated again in ethanol for 5 min, and then dried at 60°C. For the slurry preparation, 2 mg of Ag@In<sub>2</sub>O<sub>3</sub> was mixed with 300 μl ethanol and 20 μl Nafion, sonicated for 1 h. Finally, to prepare the working electrode, pre-treated NF was immersed in the slurry and oven-dried at 60°C.

### Characterization

Scanning electron microscopic analysis and Elemental mapping was carried out using SEM (JEOL JSM-6042A; Japan) while X-ray diffraction analysis was performed through (XRD, D5005 STOE and Cie GmbH Darmstadt, Germany), CuKα radiations ( $\lambda = 1.5406 \text{ \AA}$ ) at an angle ( $2\theta$ ) ranging from 10° to 80°. The FTIR Analysis were conducted on PerkinElmer, Spectrum TM100 spectrophotometer using KBr pellets in the scan range of 400–4,000  $\text{cm}^{-1}$ .

### Electrochemical Studies

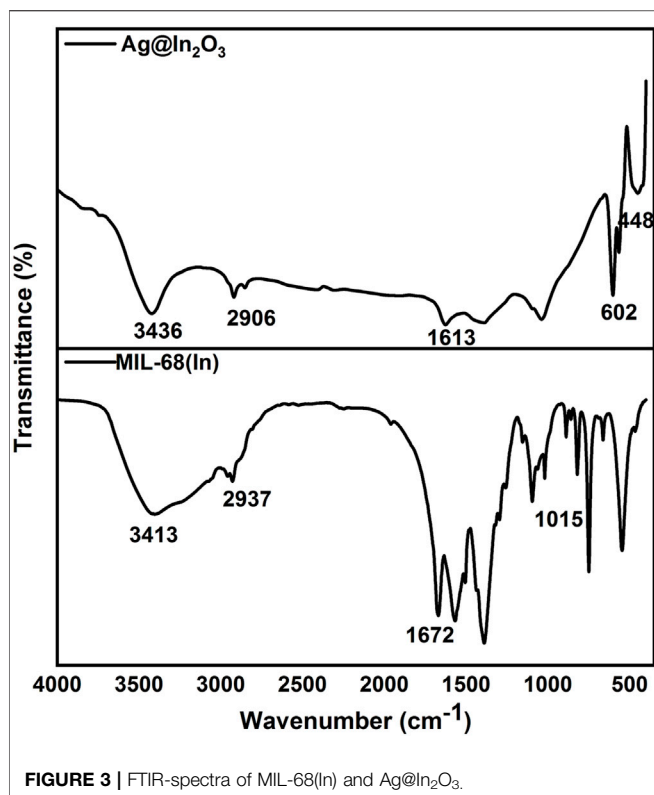
Electrochemical tests of the modified electrodes were performed using Gamry G750 electrochemical workstation. The three-electrode configuration, working electrodes were In<sub>2</sub>O<sub>3</sub> and Ag@In<sub>2</sub>O<sub>3</sub> coated on NF, a platinum (Pt) wire was used as counter electrode and Ag/AgCl as a reference electrode in 0.1 M NaOH for glucose sensing. Cyclic voltammetry for glucose sensing was performed at scan rates from 10 to 150  $\text{mVs}^{-1}$ .



## RESULTS AND DISCUSSION

### Structure Characterization

The calcination temperature has an important effect on the morphology of the MOFs-derived metal oxides. Thermogravimetric analysis (TGA) was performed by using a Discovery TGA 5500 TA instrument under an air atmosphere from 40 to 800°C, and the TGA curve of MIL-68 (In) is shown in **Figure 1**. There are two distinct stages of weight loss during the heating process. The first stage of weight loss (19%) occurs from 40 to 260°C due to the loss of adsorbed H<sub>2</sub>O, unreacted terephthalic acid and DMF. The second stage (40%) occurs in the range of 438–530°C. Such a large loss of weight is attributed to the oxidative decomposition of organic ligands in the MIL-68 (In) precursor. Thermal analysis reveal that the decomposition of



MIL-68(In) occurs in the temperature of 400–600°C. That's why the calcination temperature selected was above 600°C (Cui et al., 2018; Sun et al., 2021).

## Analytical Characterization

XRD analysis of Indium organic frameworks [MIL-68(In)] shows a high degree of crystallinity **Figure 2A** while diffraction peaks of Ag@In<sub>2</sub>O<sub>3</sub> are in perfect alignment with the JCPDS card No.06-0416. The  $2\theta$  angles at 21.4°, 30.5°, 35.4°, 37.6°, 42.6°, 45.7°, 50.1°, and 60.6° corresponds to (211), (222), (400), (411), (332), (431), (440), and (622) respectively (Tan et al., 2015). It is pertinent to mention that diffraction peaks for Ag in the XRD pattern are capped by peaks of In<sub>2</sub>O<sub>3</sub> due to low weight percentage. The prominent peaks of Ag at 38° (111) (Mohammadzadeh Kakhki et al., 2019) and 44° (200) are overlapped, although a minor peak at 64° which corresponds to (220) is observed highlighted in **Figures 2**, XRD of the In<sub>2</sub>O<sub>3</sub>. All intense peaks in the spectrum can be well indexed to cubic In<sub>2</sub>O<sub>3</sub> (JCPDS Card No. 06-0416, space group Ia3 (206), a = 10.118 Å) (Kim et al., 2011; Prasad et al., 2021).

The molecular structure of MIL-68(In)-X has been investigated by FTIR measurement. As displayed in **Figure 3** MIL-68(In) absorption bands are related to the vibrations of the organic unit (terephthalate). Bands ranging from 700 to 900 cm<sup>-1</sup> are associated with benzene ring out of plane bending. The in plane bending of the benzene ring is shown by the peak at 1,015 cm<sup>-1</sup>. Peaks near 1,400 and 1,600 cm<sup>-1</sup> represent the symmetric and asymmetric stretching modes of carboxylate structures attached to Indium centers, respectively. (Hu et al.,

2015). In Ag@In<sub>2</sub>O<sub>3</sub>, the absorption bands in the range of 448–600 cm<sup>-1</sup> shows the characteristic peaks of In-O phonon vibrations of cubic phase In<sub>2</sub>O<sub>3</sub> (Almontasser and Parveen, 2020). 3,436 cm<sup>-1</sup> shows OH stretching and 1,613 cm<sup>-1</sup> are assigned to nitrate group and shows bend deformation of water (Kulkarni and Patil, 2016). For morphological characterization of the samples, scanning electron microscopy (SEM) was performed, which indicates rod-shaped crystals with smooth surface of uncalcined MIL-68(In) **Figures 4A,B**. Because their three-dimensional networks depict a Kagom'e-like lattice with endless chains of octahedral units linked through the terephthalate ligand delimiting triangular and hexagonal channels, hexagonal symmetrical morphologies can be seen in every image. (Cui et al., 2018). **Figure 4C** shows the products obtained after the pyrolysis of MOF at 650°C. It can be observed that MIL-68(In) converted into its derived metal oxide. The loss of regular shape of the single crystal after annealing should be caused by grinding process (Xue et al., 2017).

Furthermore, the morphology of Ag@In<sub>2</sub>O<sub>3</sub> indicates its homogeneous coverage over the surface of Ni-foam **Figures 4D-F**. The existence of Ag particles was proved by the EDX patterns in **Figure 5**.

## Cyclic Voltammetric Studies

Cyclic Voltammetry was used to determine the modified electrode's electrochemical behavior toward glucose in the potential range of 0 to + 0.8 V. **Figure 6A** shows cyclic voltammograms of bare Ni-foam and Ag@In<sub>2</sub>O<sub>3</sub> with and without glucose at a scan rate of 50 mVs<sup>-1</sup>. In **Figure 6A**, bare Ni-foam shows no response in the absence of glucose, but a small peak of 4.5 mA was observed at + 0.55 V in the presence of glucose.

A pair of redox peaks observed in CV curves suggest the presence of reversible Faradaic reaction of Ni<sup>2+</sup>/Ni<sup>3+</sup> with the assistance of OH<sup>-</sup> (Wang et al., 2002). Although bare NF showed electro-oxidation towards glucose, responses are weak. However, when glucose is present, Ag@In<sub>2</sub>O<sub>3</sub> modified electrode showed a peak at 25.2 mA at + 0.65 V. To demonstrate the effect of composite, In<sub>2</sub>O<sub>3</sub> and Ag@In<sub>2</sub>O<sub>3</sub> were compared in **Figure 6B**, and it is evident from the figure that entrapment of Ag in metal oxide increase its catalytic activity. A visible difference in the peaks currents for both electrodes can be observed. A relatively high current response of 25.6 mA at + 0.68 V was achieved by Ag@In<sub>2</sub>O<sub>3</sub> modified electrode compared to In<sub>2</sub>O<sub>3</sub> which showed peak current of 9.2 mA at + 0.66 V. This improved performance is the result of the perfect combination of mesoporous structure of metal oxide and Ag and their synergistic effect for the catalytic behavior. The behavior of Ag@In<sub>2</sub>O<sub>3</sub> modified electrode against various glucose concentrations is shown in **Figure 6C**. This can be easily seen that by increasing the concentration of glucose from 2 to 8 mM, oxidation current increases, indicating a superior electrocatalytic behavior of Ag@In<sub>2</sub>O<sub>3</sub> modified NF. However, after 8 mM concentration of glucose, a constant response was observed, indicating the saturation state of analyte. Investigation of the effect of potential scan rate in 0.1 M NaOH solution containing 2 mM glucose ranging from 10 to 150 mVs<sup>-1</sup>

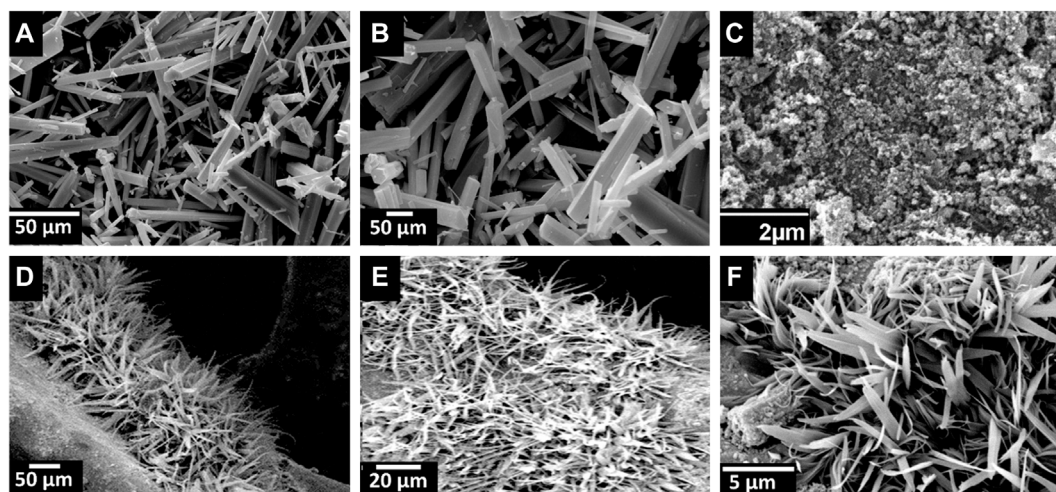


**FIGURE 4** | SEM micrographs of MIL-68(In) is shown in (A) and (B). Figure 4(C) is Ag@In<sub>2</sub>O<sub>3</sub> and (D–F) shows Ag@In<sub>2</sub>O<sub>3</sub> coated on NF.

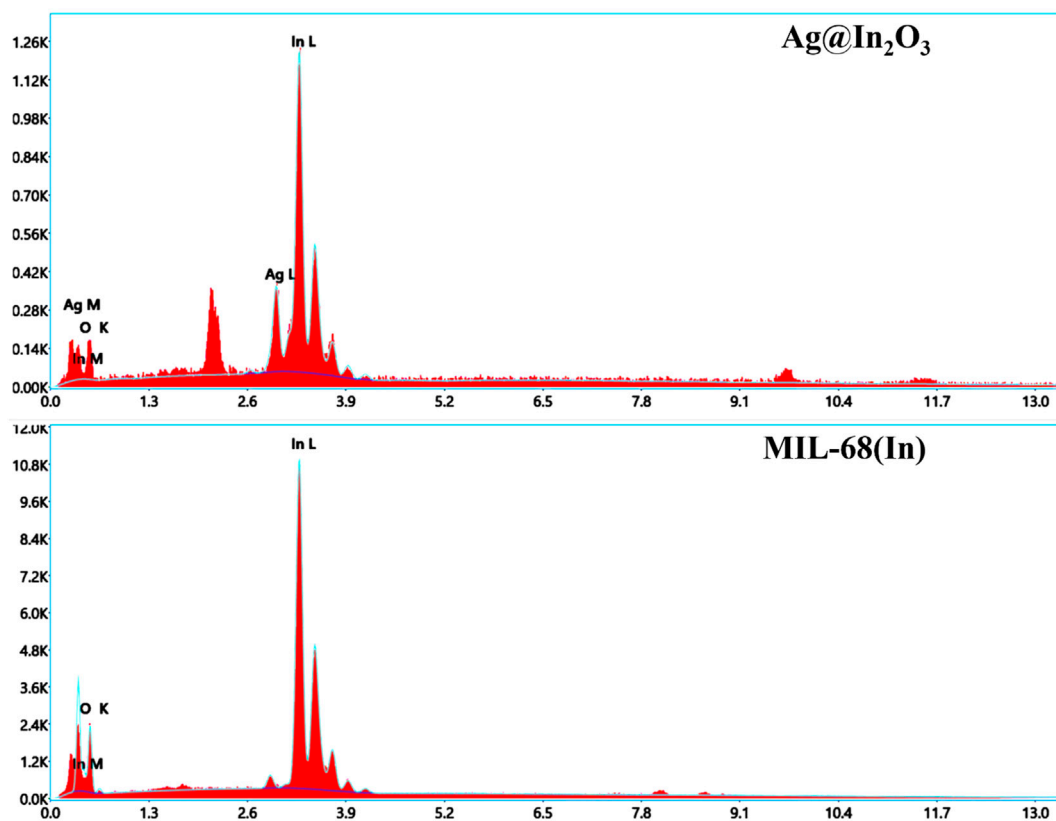


**FIGURE 5** | EDS analysis of MIL-68(In) and Ag@In<sub>2</sub>O<sub>3</sub>.

shows the mechanism involved in the electrochemical process on electrode surface. **Figure 6D** shows the scan rate on the glucose oxidation for Ag@In<sub>2</sub>O<sub>3</sub>. With the increase in scan rate, the glucose oxidation current is increased along with a shift of anodic

peaks towards positive range of the potential window +0.49 to +0.75 V, while cathodic peaks shifted towards negative potential from 0.28 to 0.09 V. This behavior suggests that the process for glucose oxidation is diffusion controlled. It can further be

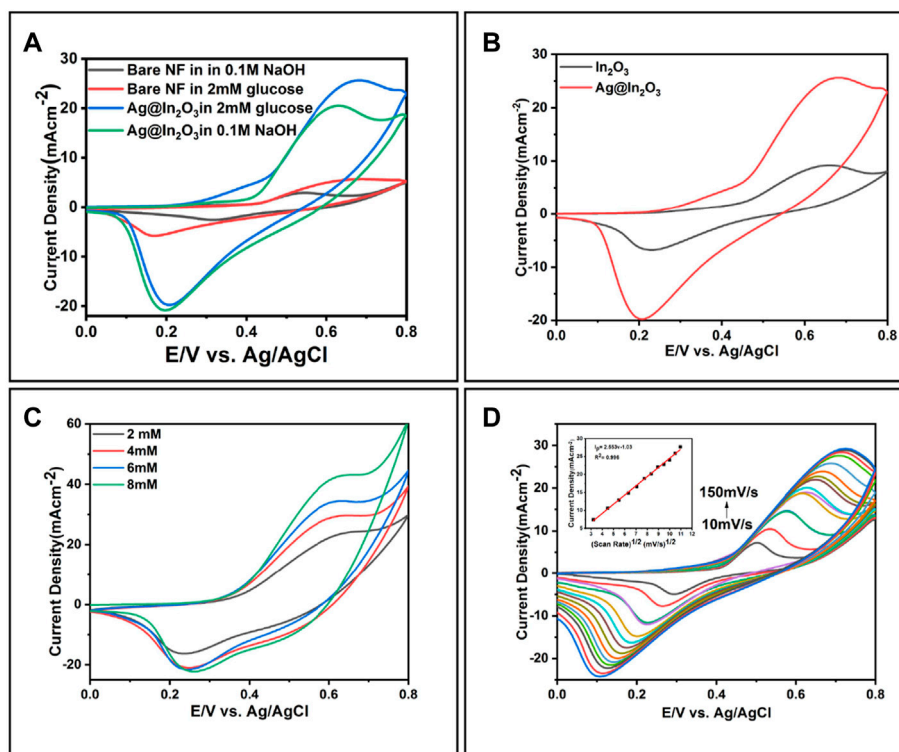


**FIGURE 6 | (A)** Cyclic Voltammetry of bare NF and Ag@In<sub>2</sub>O<sub>3</sub> in 0.1 M NaOH, with and without glucose **(B)** Comparison between the CVs of In<sub>2</sub>O<sub>3</sub> and Ag@In<sub>2</sub>O<sub>3</sub> in 2 mM glucose, **(C)** Response of Ag@In<sub>2</sub>O<sub>3</sub> modified NF after successive addition of 2–8 mM glucose, **(D)** CVs of Ag@In<sub>2</sub>O<sub>3</sub> in the presence of 2 mM glucose in the potential range of 0 V to +0.8 V at different scan rates of 10–150 mVs<sup>-1</sup> (Inset: the plot of  $I_p$  vs.  $v$ ).

postulated that metal oxide (In<sub>2</sub>O<sub>3</sub>) oxidizes glucose into the gluconic acid and reduced to its lower oxidation state (In<sub>2</sub>O) followed by its reaction with the alkaline electrolyte (hydroxyl ion) and conversion back to In<sub>2</sub>O<sub>3</sub> and water. This oxidation process of glucose is enhanced by the synergistic effect of Ag located nearby metal oxide. Inset of **Figure 6D** depicts a linearity graph between anodic peak potential and the square root of the scan rates, which indicates the kinetic limitation of the reaction between redox sites of the Ag@In<sub>2</sub>O<sub>3</sub> modified electrode and the analyte (Liu et al., 2017).

## Amperometric Studies

For amperometric studies, first step is to analyze the optimized potential because the detection potential strongly influences amperometric response of biosensors. Chronoamperometry determines sensitivity, response, and linear range of the modified electrodes.

**Figure 7A** shows *i-t* curve for bare NF and Ag@In<sub>2</sub>O<sub>3</sub> modified NF. It is evident from the results that current responses obtained for Ag@In<sub>2</sub>O<sub>3</sub> modified electrode were prominent while no stepwise linear increase in the current responses could be observed for bare NF. This is in line with the CV graphs. Similarly, **Figure 7B** depicts the comparison between Ag@In<sub>2</sub>O<sub>3</sub> and In<sub>2</sub>O<sub>3</sub> modified electrodes and it is observed that the response of oxidation currents in In<sub>2</sub>O<sub>3</sub> modified electrode is less as compared to Ag@In<sub>2</sub>O<sub>3</sub>. The

initial oxidation current response of In<sub>2</sub>O<sub>3</sub> was 1.9 mA when 10 μM glucose was added. **Figure 7C** shows the amperogram of Ag@In<sub>2</sub>O<sub>3</sub> modified electrode obtained by adding various known glucose concentrations into the stirring solution of 0.1 M NaOH at the potential of +0.7 V. The initial oxidation current response of 10.9 mA was achieved by adding 10 μM glucose. The oxidation current of the glucose linearly increased with the increasing glucose concentrations, giving broad linear range from 10 to 2,162 μM with a correlation coefficient of 0.978 and 0.997. Response time of the sensing material against the analyte concentration is crucial for assessing the performance of an electrochemical sensor. **Figure 7C**, inset shows the amplified view of the response time attained upon analyte addition. It can be seen that after adding glucose, the current reached its steady state within 3 s.

Better performance of Ag@In<sub>2</sub>O<sub>3</sub> modified electrode could be associated with increased surface area, better catalytic activity, and high conductivity as a result of synergistic effect of Ag and Indium oxide in a nanocomposite. In response to various glucose concentrations, **Figure 7D** shows two wide linear ranges of oxidative currents. One region is from 10 μM to 0.8 mM and the other range is from 0.8 to 2.16 mM. From **Figure 7D**, for 10 μM to 0.8 mM range:  $I_p = 0.0033C + 11.0$  ( $R^2 = 0.978$ )

While for 0.8–2.16 mM range:  $I_p = 0.00155C + 12.13$  ( $R^2 = 0.997$ )

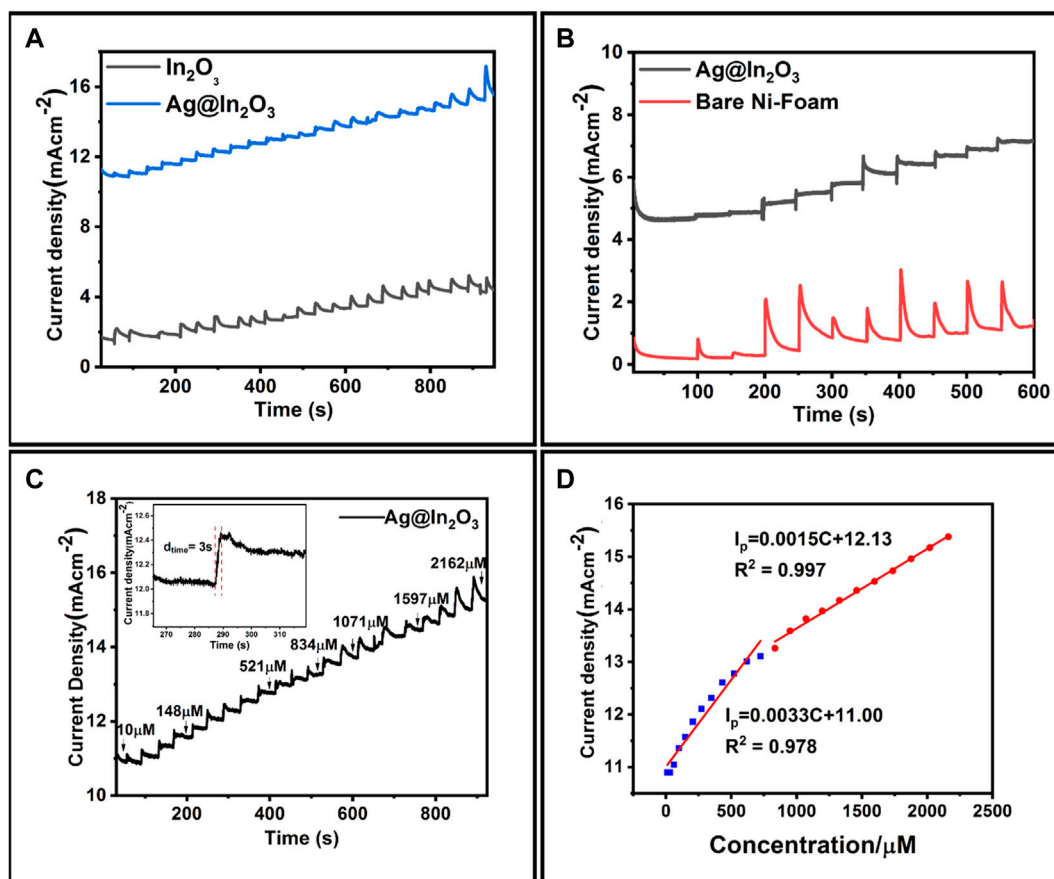


**FIGURE 7 |** (A) Amperograms of Bare NF and Ag@In<sub>2</sub>O<sub>3</sub> in NaOH (0.1 M) stirred solution with different glucose concentrations, (B) Amperograms of In<sub>2</sub>O<sub>3</sub> and Ag@In<sub>2</sub>O<sub>3</sub>, (C) Amperogram of Ag@In<sub>2</sub>O<sub>3</sub> modified NF at +0.7 V obtained from the stepwise additions of various glucose concentrations (30 µl after every 40 s interval) in the range of 10–2200 µM (inset: magnified amperogram showing current response of 3 s), (D) Two linear ranges at +0.7 V of calibration curve between glucose concentration and current response.

**TABLE 1 |** Comparison of modified electrode with other metal oxides based electrochemical sensors for glucose sensing.

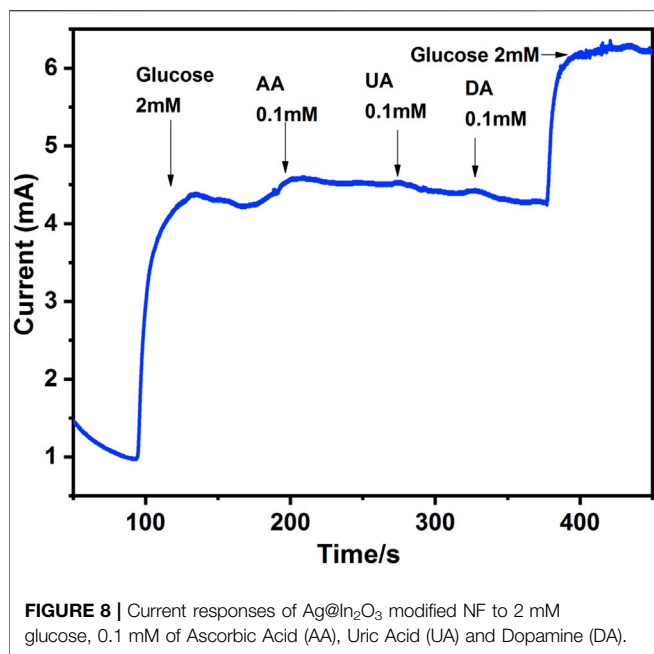
Year	Electrode composition	Sensitivity mA mM <sup>-1</sup> cm <sup>-2</sup>	Linear range	Detection limit	References
2020	Co <sub>3</sub> (BTC) <sub>2</sub> MOFs/GCE	1.792 and 1.002	1 µM to 0.33 mM and 0.33–1.38 mM	0.33 µM	Shahrokhian et al. (2020)
2020	Co doped Cu-MOF/Cu <sub>2</sub> O Nanorods/Cu foam	0.0119	0.001–1.07 mM	0.72 µM	Wei et al. (2020)
2019	Co-ZIF/NF	2.981	10–120 mM	0.42 mM	Arul and John, (2019)
2019	Co-MOF/NF	10.886	0.001–3 mM	1.3 nM	Li et al. (2019c)
2017	Ni@C/Ni foam	32.79	0.15 µM–1.48 mM	50 nM	Zhang et al. (2017)
<b>2021</b>	<b>Ag@In<sub>2</sub>O<sub>3</sub>/NF</b>	<b>1.51 and 3.31</b>	<b>10 µM to 0.8 mM and 0.8 mM to 2.16 mM</b>	<b>0.49 µM</b>	<b>This work</b>

Bold values mention the values extracted from the current work.

The sensitivity values obtained from Ag@In<sub>2</sub>O<sub>3</sub> modified electrode are 3.31 mA mM<sup>-1</sup> cm<sup>-2</sup> and 1.51 mA mM<sup>-1</sup> cm<sup>-2</sup> from first and second linear ranges, respectively. The limit of detection calculation is based on the signal to noise ratio ( $S/N = 3$ ). We could also state that the lower detection limit is an experimental value, reflecting the minimal amount of glucose addition required to elicit a response from the electrode. The calculated detection limit is 0.49 µM by using the formula  $LOD =$

$(3 \times \text{noise current density})/\text{sensitivity}$ . The limit of quantification is 1.617 µM (Dayakar et al., 2018).

The possible explanation behind the difference in two slopes of the calibration curve is the absorption of intermediates produced during the glucose oxidation on the electrode surface (Luo et al., 2012). Furthermore, after successive administrations of glucose at high concentrations, a minor baseline drift in the amperogram is



detected, which could be related to slight variations in local pH, faster glucose consumption than its diffusion, or the adsorption of intermediates on the active sites (Chen et al., 2014).

Table 1 compares our Ag@In<sub>2</sub>O<sub>3</sub> modified electrode with other metal oxides based electrochemical sensors used for glucose sensing in the literature.

### Interference Study

Another crucial analytical factor determined by amperometric experiments is differentiating glucose in blood among other electroactive species. Glucose concentration in blood lies between 4–7 mM, depending on the physiological condition of the person (Arif et al., 2020). Certain interfering species are present along with glucose in the blood with 30–50 times less concentration than glucose, but their presence can influence glucose detection. Therefore, it is essential to assess the sensor's selectivity towards glucose (El Khatib and Abdel Hameed, 2011). Interfering agents that commonly co-exist with glucose in biological systems are uric acid (UA), dopamine (DA) and acetaminophen (AP). Figure 8 shows the response curve of the selectivity of modified electrode towards glucose. When glucose was added into 0.1 M NaOH solution, a visible peak current appeared while minimum response was shown when 0.1 mM concentration of interfering agents such as AA, UA and DA were introduced in the system. The response

curve signifies that Ag@In<sub>2</sub>O<sub>3</sub> modified electrode has good selectivity towards glucose.

### Stability and Reproducibility

Electrochemical sensor reproducibility and stability are essential parameters for practical applications. Similarly, the amperometric responses from Ag@In<sub>2</sub>O<sub>3</sub> NF five electrodes had an RSD of 2.47%, which was satisfactory. The current response to 30 μM glucose was tested for 5 days to investigate the stability of the Ag@In<sub>2</sub>O<sub>3</sub> NF electrode after storage at ambient temperature in air. A 3.45% RSD value was achieved.

### CONCLUSION

In the present investigation, an electrochemical sensor based on Ag decorated metal oxide frameworks to determine the electrocatalytic activity of glucose is demonstrated. The Ag@In<sub>2</sub>O<sub>3</sub> showed enhanced activity compared to the pure metal oxide because of more electroactive sites, large surface to volume ratio, and fast catalytic activity because of the electrical conductivity provided by Ag<sup>+</sup> in the nanocomposite. The as prepared sensor showed remarkable sensitivity values 3.31 and 1.51 mA mM<sup>-1</sup> cm<sup>-2</sup> for the two linear ranges of 10 μM–0.8 mM and 0.8–2.16 mM, with response time of 3 s and 0.49 μM detection limit.

### DATA AVAILABILITY STATEMENT

The original contributions presented in the study are included in the article/Supplementary Material, further inquiries can be directed to the corresponding author.

### AUTHOR CONTRIBUTIONS

DA: experimentation, data curation, interpretation of results, drafting of manuscript ZH: conceptualization, supervision, revision and proofreading of the manuscript AA: data curation, interpretation of results MS: financial support, interpretation of results, proof reading of manuscript.

### ACKNOWLEDGMENTS

This research was conducted at the School of Chemical and Materials Engineering (SCME), National University of Sciences and Technology, Sector H-12, Islamabad. ZH acknowledges the financial and administrative support from the SCME, NUST.

### REFERENCES

- Almontasser, A., and Parveen, A. (2020). Synthesis and Characterization of Indium Oxide Nanoparticles. *AIP Conf. Proc.* 2220, 20191. doi:10.1063/5.0001683
- Arif, D., Hussain, Z., Sohail, M., Liaqat, M. A., Khan, M. A., and Noor, T. (2020). A Non-enzymatic Electrochemical Sensor for Glucose Detection Based on Ag@

- TiO<sub>2</sub>@ Metal-Organic Framework (ZIF-67) Nanocomposite. *Front. Chem.* 8, 573510. doi:10.3389/fchem.2020.573510

- Arul, P., and John, S. A. (2019). Organic Solvent Free *In Situ* Growth of Flower like Co-ZIF Microstructures on Nickel Foam for Glucose Sensing and Supercapacitor Applications. *Electrochimica Acta* 306, 254–263. doi:10.1016/j.electacta.2019.03.117
- Barthelet, K., Marrot, J., Férey, G., and Riou, D. (2004). VIII(OH){O<sub>2</sub>C-C<sub>6</sub>H<sub>4</sub>-CO<sub>2</sub>}.(HO<sub>2</sub>C-C<sub>6</sub>H<sub>4</sub>-CO<sub>2</sub>H)<sub>x</sub>(DMF)<sub>y</sub>(H<sub>2</sub>O)<sub>z</sub> (Or MIL-68), a New

- Vanadocarboxylate with a Large Pore Hybrid Topology : Reticular Synthesis with Infinite Inorganic Building Blocks? *Chem. Commun.* 4, 520–521. doi:10.1039/B312589K
- Cao, X., Tan, C., Sindoro, M., and Zhang, H. (2017). Hybrid Micro-/nano-structures Derived from Metal-Organic Frameworks: Preparation and Applications in Energy Storage and Conversion. *Chem. Soc. Rev.* 46, 2660–2677. doi:10.1039/c6cs00426a
- Chen, T., Li, X., Qiu, C., Zhu, W., Ma, H., and Chen, S. (2014). Electrochemical Sensing of Glucose by Carbon Cloth-Supported Co<sub>3</sub>O<sub>4</sub>/PbO<sub>2</sub> Core-Shell Nanorod Arrays. *Biosens. Bioelectron.* 53, 200–206. doi:10.1016/j.bios.2013.09.059
- Chu, D., Li, F., Song, X., Ma, H., Tan, L., Pang, H., et al. (2020). A Novel Dual-Tasking Hollow Cube NiFe<sub>2</sub>O<sub>4</sub>-NiCo-LDH@rGO Hierarchical Material for High Performance Supercapacitor and Glucose Sensor. *J. Colloid Interface Sci.* 568, 130–138. doi:10.1016/j.jcis.2020.02.012
- Clark, L. C., and Lyons, C. (1962). Electrode Systems for Continuous Monitoring in Cardiovascular Surgery. *Ann. N. Y. Acad. Sci.* 102, 29–45. doi:10.1111/j.1749-6632.1962.tb13623.x
- Cui, Y. F., Jiang, W., Liang, S., Zhu, L. F., and Yao, Y. W. (2018). MOF-derived Synthesis of Mesoporous In/Ga Oxides and Their Ultra-sensitive Ethanol-Sensing Properties. *J. Mat. Chem. A* 6, 14930–14938. doi:10.1039/C8TA00269J
- Dayakar, T., Venkateswara Rao, K., Vinodkumar, M., Bikshalu, K., and Ramachandra, R. K. (2018). Novel Synthesis and Characterization of Ag@TiO<sub>2</sub> Core Shell Nanostructure for Non-enzymatic Glucose Sensor. *Appl. Surf. Sci.* 435, 216–224. doi:10.1016/j.apsusc.2017.11.077
- El Khatib, K. M., and Abdel Hameed, R. M. (2011). Development of Cu<sub>2</sub>O/Carbon Vulcan XC-72 as Non-enzymatic Sensor for Glucose Determination. *Biosens. Bioelectron.* 26, 3542–3548. doi:10.1016/j.bios.2011.01.042
- Govindasamy, M., Wang, S. F., Subramanian, B., Ramalingam, R. J., Al-lohedan, H., and Sathiyam, A. (2019). A Novel Electrochemical Sensor for Determination of DNA Damage Biomarker (8-Hydroxy-2'-Deoxyguanosine) in Urine Using Sonochemically Derived Graphene Oxide Sheets Covered Zinc Oxide Flower Modified Electrode. *Ultrason. Sonochem.* 58, 104622. doi:10.1016/j.ultrsonch.2019.104622
- Hu, Y., Lin, B., He, P., Li, Y., Huang, Y., and Song, Y. (2015). Probing the Structural Stability of and Enhanced CO<sub>2</sub> Storage in MOF MIL-68(In) under High Pressures by FTIR Spectroscopy. *Chemistry* 21, 18739–18748. doi:10.1002/CHEM.201502980
- Hwang, D. W., Lee, S., Seo, M., and Chung, T. D. (2018). Recent Advances in Electrochemical Non-enzymatic Glucose Sensors – A Review. *Anal. Chim. Acta* 1033, 1–34. doi:10.1016/j.aca.2018.05.051
- Kim, H. S., Na, H. G., Yang, J. C., Lee, C., and Kim, H. W. (2011). Synthesis, Structure, Photoluminescence, and Raman Spectrum of Indium Oxide Nanowires. 119:143–145. doi:10.12693/aphyspola.119.143
- Kulkarni, S. C., and Patil, D. S. (2016). Synthesis and Characterization of Uniform Spherical Shape Nanoparticles of Indium Oxide. *J. Mat. Sci. Mat. Electron.* 27, 3731–3735. doi:10.1007/S10854-015-4215-5
- Li, J., Yu, C., Wu, Y.-n., Zhu, Y., Xu, J., Wang, Y., et al. (2019a). Novel Sensing Platform Based on Gold Nanoparticle-Aptamer and Fe-Metal-Organic Framework for Multiple Antibiotic Detection and Signal Amplification. *Environ. Int.* 125, 135–141. doi:10.1016/j.envint.2019.01.033
- Li, L., Liu, Y., Ai, L., and Jiang, J. (2019b). Synthesis of the Crystalline Porous Copper Oxide Architectures Derived from Metal-Organic Framework for Electrocatalytic Oxidation and Sensitive Detection of Glucose. *J. Ind. Eng. Chem.* 70, 330–337. doi:10.1016/j.jiec.2018.10.033
- Li, Y., Xie, M., Zhang, X., Liu, Q., Lin, D., Xu, C., et al. (2019c). Co-MOF Nanosheet Array: A High-Performance Electrochemical Sensor for Non-enzymatic Glucose Detection. *Sensors Actuators, B Chem.* 278, 126–132. doi:10.1016/j.snb.2018.09.076
- Liang, Q., Xu, H., Zhao, J., and Gao, S. (2012). Micro Humidity Sensors Based on ZnO-In<sub>2</sub>O<sub>3</sub> 2O<sub>3</sub> Thin Films with High Performances. *Sensors Actuators, B Chem.* 165, 76–81. doi:10.1016/j.snb.2012.02.019
- Liu, M., Zhang, S., Gao, J., Qian, Y., Song, H., Wang, S., et al. (2017). Enhanced Electrocatalytic Nitrite Determination Using Poly(diallyldimethylammonium Chloride)-Coated Fe<sub>1.833</sub>(OH)<sub>0.5</sub>O<sub>2.5</sub>-decorated N-Doped Graphene Ternary Hierarchical Nanocomposite. *Sensors Actuators, B Chem.* 243, 184–194. doi:10.1016/j.snb.2016.11.124
- Lü, Y., Zhan, W., He, Y., Wang, Y., Kong, X., Kuang, Q., et al. (2014). MOF-templated Synthesis of Porous Co<sub>3</sub>O<sub>4</sub> Concave Nanocubes with High Specific Surface Area and Their Gas Sensing Properties. *ACS Appl. Mat. Interfaces* 6, 4186–4195. doi:10.1021/am405858v
- Luo, J., Jiang, S., Zhang, H., Jiang, J., and Liu, X. (2012). A Novel Non-enzymatic Glucose Sensor Based on Cu Nanoparticle Modified Graphene Sheets Electrode. *Anal. Chim. Acta* 709, 47–53. doi:10.1016/j.aca.2011.10.025
- Mohammadzadeh Kakhki, R., Hedayat, S., and Mohammadzadeh, K. (2019). Novel, Green and Low Cost Synthesis of Ag Nanoparticles with Superior Adsorption and Solar Based Photocatalytic Activity. *J. Mat. Sci. Mat. Electron.* doi:10.1007/S10854-019-01203-5
- Nichols, S. P., Koh, A., Storm, W. L., Shin, J. H., and Schoenfish, M. H. (2013). Biocompatible Materials for Continuous Glucose Monitoring Devices. *Chem. Rev.* 113, 2528–2549. doi:10.1021/cr300387j
- Prasad, K. H., Kumar, K. D. A., Mele, P., Christy, A. J., Gunavathy, K. V., Alomairy, S., et al. (2021). Structural, Magnetic and Gas Sensing Activity of Pure and Cr Doped In<sub>2</sub>O<sub>3</sub> Thin Films Grown by Pulsed Laser Deposition. *Coatings* 11, 588. doi:10.3390/COATINGS11050588
- Salunkhe, R. R., Kaneti, Y. V., and Yamauchi, Y. (2017). Metal-Organic Framework-Derived Nanoporous Metal Oxides toward Supercapacitor Applications: Progress and Prospects. *ACS Nano* 11, 5293–5308. doi:10.1021/acsnano.7b02796
- Shahrokhian, S., Ezzati, M., and Hosseini, H. (2020). Fabrication of a Sensitive and Fast Response Electrochemical Glucose Sensing Platform Based on Co-based Metal-Organic Frameworks Obtained from Rapid *In Situ* Conversion of Electrodeposited Cobalt Hydroxide Intermediates. *Talanta* 210, 120696. doi:10.1016/j.talanta.2019.120696
- Sheng, Q., Liu, D., and Zheng, J. (2016). NiCo Alloy Nanoparticles Anchored on Polypyrrole/reduced Graphene Oxide Nanocomposites for Nonenzymatic Glucose Sensing. *New J. Chem.* 40, 6658–6665. doi:10.1039/c6nj01264g
- Song, W. J. (2017). Intracellular DNA and microRNA Sensing Based on Metal-Organic Framework Nanosheets with Enzyme-free Signal Amplification. *Talanta* 170, 74–80. doi:10.1016/j.talanta.2017.02.040
- Song, X. Z., Meng, Y. L., Chen, X., Sun, K. M., and Wang, X. F. (2018). Hollow NiFe<sub>2</sub>O<sub>4</sub> Hexagonal Bipyramids for High-Performance: N-Propanol Sensing at Low Temperature. *New J. Chem.* 42, 14071–14074. doi:10.1039/c8nj02438c
- Song, Y., Wei, C., He, J., Li, X., Lu, X., and Wang, L. (2015). Porous Co nanobeads/rGO Nanocomposites Derived from rGO/Co-Metal Organic Frameworks for Glucose Sensing. *Sensors Actuators, B Chem.* 220, 1056–1063. doi:10.1016/j.snb.2015.06.052
- Stock, N., and Biswas, S. (2012). Synthesis of Metal-Organic Frameworks (MOFs): Routes to Various MOF Topologies, Morphologies, and Composites. *Chem. Rev.* 112, 933–969. doi:10.1021/cr200304e
- Sun, C., Gao, L., Wang, D., Zhang, M., Liu, Y., Geng, Z., et al. (2016). Biocompatible Polypyrrole-Block Copolymer-Gold Nanoparticles Platform for Determination of Inosine Monophosphate with Bi-enzyme Biosensor. *Sensors Actuators, B Chem.* 230, 521–527. doi:10.1016/j.snb.2016.02.111
- Sun, Y., Dong, Z., Zhang, D., Zeng, Z., Zhao, H., An, B., et al. (2021). The Fabrication and Triethylamine Sensing Performance of In-MIL-68 Derived In<sub>2</sub>O<sub>3</sub> with Porous Lacunaris Structure. *Sensors Actuators, B Chem.* 326, 128791. doi:10.1016/j.snb.2020.128791
- Tan, S., Gil, L. B., Subramanian, N., Sholl, D. S., Nair, S., Jones, C. W., et al. (2015). Catalytic Propane Dehydrogenation over In<sub>2</sub>O<sub>3</sub>-Ga<sub>2</sub>O<sub>3</sub> Mixed Oxides. *Appl. Catal. A Gen.* 498, 167–175. doi:10.1016/j.apcata.2015.03.020
- Volklinger, C., Meddouri, M., Loiseau, T., Guillou, N., Marrot, J., Férey, G., et al. (2008). The Kagomé Topology of the Gallium and Indium Metal-Organic Framework Types with a MIL-68 Structure: Synthesis, XRD, Solid-State NMR Characterizations, and Hydrogen Adsorption. *Inorg. Chem.* 47, 11892–11901. doi:10.1021/ic801624v
- Wang, J. (2008). Electrochemical Glucose Biosensors. *Chem. Rev.* 108, 814–825. doi:10.1021/cr068123a
- Wang, J., Zhao, J., Yang, J., Cheng, J., Tan, Y., Feng, H., et al. (2020a). An Electrochemical Sensor Based on MOF-Derived NiO@ZnO Hollow Microspheres for Isoniazid Determination. *Microchim. Acta* 187, 1–8. doi:10.1007/s00604-020-04305-8
- Wang, L., Xie, Y., Wei, C., Lu, X., Li, X., and Song, Y. (2015). Hierarchical NiO Superstructures/Foam Ni Electrode Derived from Ni Metal-Organic

- Framework Flakes on Foam Ni for Glucose Sensing. *Electrochim. Acta* 174, 846–852. doi:10.1016/j.electacta.2015.06.086
- Wang, S., Guan, B. Y., and Lou, X. W. D. (2018). Construction of ZnIn<sub>2</sub>S<sub>4</sub>-In<sub>2</sub>O<sub>3</sub> Hierarchical Tubular Heterostructures for Efficient CO<sub>2</sub> Photoreduction. *J. Am. Chem. Soc.* 140, 5037–5040. doi:10.1021/JACS.8B02200/SUPPL\_FILE/JA8B02200\_SI\_001.PDF
- Wang, S., Xiao, B., Yang, T., Wang, P., Xiao, C., Li, Z., et al. (2014). Enhanced HCHO Gas Sensing Properties by Ag-Loaded Sunflower-like in 2O<sub>3</sub> Hierarchical Nanostructures. *J. Mat. Chem. A* 2, 6598–6604. doi:10.1039/c3ta15110g
- Wang, X., Wang, T., Si, G., Li, Y., Zhang, S., Deng, X., et al. (2020b). Oxygen Vacancy Defects Engineering on Ce-Doped  $\alpha$ -Fe<sub>2</sub>O<sub>3</sub> Gas Sensor for Reducing Gases. *Sensors Actuators, B Chem.* 302. doi:10.1016/J.SNB.2019.127165
- Wang, Y. de., Ma, C. L., Sun, X. D., and Li, H. De. (2002). Preparation of Nanocrystalline Metal Oxide Powders with the Surfactant-Mediated Method. *Inorg. Chem. Commun.* 5, 751–755. doi:10.1016/S1387-7003(02)00546-4
- Wei, C., Li, X., Xiang, W., Yu, Z., and Liu, Q. (2020). MOF Derived Seaweed-like CoCu Oxides Nanorod Arrays for Electrochemical Non-enzymatic Glucose Sensing with Ultrahigh Sensitivity. *Sensors Actuators, B Chem.* 324, 128773. doi:10.1016/j.snb.2020.128773
- Xue, Y.-Y., Wang, J.-L., Li, S.-N., Jiang, Y.-C., Hu, M.-C., and Zhai, Q.-G. (2017). Mesoporous Ag/In<sub>2</sub>O<sub>3</sub> Composite Derived from Indium Organic Framework as High Performance Formaldehyde Sensor. *J. Solid State Chem.* 251, 170–175. doi:10.1016/J.JSSC.2017.04.024
- Yang, Y., and Gao, W. (2019). Wearable and Flexible Electronics for Continuous Molecular Monitoring. *Chem. Soc. Rev.* 48, 1465–1491. doi:10.1039/c7cs00730b
- Zhan, B., Liu, C., Chen, H., Shi, H., Wang, L., Chen, P., et al. (2014). Free-standing Electrochemical Electrode Based on Ni(OH)<sub>2</sub>/3D Graphene Foam for Nonenzymatic Glucose Detection. *Nanoscale* 6, 7424–7429. doi:10.1039/c4nr01611d
- Zhang, D., Yang, Z., Li, P., and Zhou, X. (2019). Ozone Gas Sensing Properties of Metal-Organic Frameworks-Derived In<sub>2</sub>O<sub>3</sub> Hollow Microtubes Decorated with ZnO Nanoparticles. *Sensors Actuators, B Chem.* 301. doi:10.1016/J.SNB.2019.127081
- Zhang, L., Ding, Y., Li, R., Ye, C., Zhao, G., and Wang, Y. (2017). Ni-Based Metal-Organic Framework Derived Ni@C Nanosheets on a Ni Foam Substrate as a Supersensitive Non-enzymatic Glucose Sensor. *J. Mat. Chem. B* 5, 5549–5555. doi:10.1039/c7tb01363a
- Zhao, J., Lin, Y., Wu, J., Nyein, H. Y. Y., Bariya, M., Tai, L. C., et al. (2019). A Fully Integrated and Self-Powered Smartwatch for Continuous Sweat Glucose Monitoring. *ACS Sensors* 4, 1925–1933. doi:10.1021/acssensors.9b00891
- Zhou, C., Zhang, Y., Li, Y., and Liu, J. (2013). Construction of High-Capacitance 3D CoO@Polypyrrole Nanowire Array Electrode for Aqueous Asymmetric Supercapacitor. *Nano Lett.* 13, 2078–2085. doi:10.1021/nl400378j

**Conflict of Interest:** The authors declare that the research was conducted in the absence of any commercial or financial relationships that could be construed as a potential conflict of interest.

**Publisher's Note:** All claims expressed in this article are solely those of the authors and do not necessarily represent those of their affiliated organizations, or those of the publisher, the editors and the reviewers. Any product that may be evaluated in this article, or claim that may be made by its manufacturer, is not guaranteed or endorsed by the publisher.

Copyright © 2022 Arif, Hussain, Abbasi and Sohail. This is an open-access article distributed under the terms of the Creative Commons Attribution License (CC BY). The use, distribution or reproduction in other forums is permitted, provided the original author(s) and the copyright owner(s) are credited and that the original publication in this journal is cited, in accordance with accepted academic practice. No use, distribution or reproduction is permitted which does not comply with these terms.